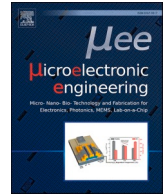




Contents lists available at ScienceDirect

Microelectronic Engineering

journal homepage: www.elsevier.com/locate/mee

Research paper

Characterization of AlN and AlScN film ICP etching for micro/nano fabrication

Zhifang Luo^{a,b,c,*}, Shuai Shao^{a,b,c}, Tao Wu^{a,*}^a School of Information Science and Technology, ShanghaiTech University, China^b Shanghai Institute of Microsystem and Information Technology, Chinese Academy of Sciences, China^c University of Chinese Academy of Sciences, China

ARTICLE INFO

Keywords:

ICP etching
Etching model
AlN
AlScN
Micro/Nano fabrication
Piezoelectric resonators

ABSTRACT

We investigate the inductively coupled plasma (ICP) etching characteristics of (0002) Aluminum Nitride (AlN) and Aluminum Scandium Nitride ($\text{Al}_{0.94}\text{Sc}_{0.06}\text{N}$) piezoelectric thin films as well as the implementation on piezoelectric lamb wave resonators. A profile of 84° is obtained on AlN thin film, with an etching rate of approximately 230 nm/min, and a selectivity of 0.77:1 relative to photoresist mask. A nearly 80° profile and over 30:1 selectivity are accomplished using Ni film as the etching mask. $\text{Al}_{0.94}\text{Sc}_{0.06}\text{N}$ film has achieved a profile of 77° by optimizing the RF power. Finally, AlN contour mode resonators (CMRs) are fabricated and characterized, and a CMR operating at about 400 MHz with a quality factor exceeding 1600 has been demonstrated.

1. Introduction

Due to the demand of electronic devices with lower cost, better performance, smaller size, and enhanced sustainability, Micro-electromechanical Systems (MEMS) transducers are one of the main next generation technology candidates that benefit from miniaturization [1–3]. The piezoelectric MEMS resonators, with a high quality factor and a large electromechanical coupling, are promising products in Radio Frequency (RF) systems [4–8]. The main materials for piezoelectric MEMS resonators are Aluminum Nitride (AlN), piezoelectric ceramics (PZT), Zinc Oxide (ZnO) and Lithium Niobate (LN) [9–13]. In recent years, doped AlN films, especially Aluminum Scandium Nitride (AlScN), has been studied due to its enhancement of d_{33} and d_{31} piezoelectric coefficients [14]. Thanks to their monolithic integration and superior performance, AlN and AlScN thin films based piezoelectric MEMS resonators have attracted more and more attention. There are many different kinds of MEMS resonators, such as surface acoustic wave (SAW) resonators [15,16], film bulk acoustic resonators (FBAR) [17–19]. However, SAW devices are not compatible with the CMOS process. The frequency of FBAR primarily depends on the thickness of piezoelectric layer; therefore, it is very challenging to achieve multiple operating frequencies or wide frequency tunability in one chip. On the other hand, AlN and AlScN based contour-mode resonators (CMRs) are compatible with CMOS process [20–24]. Meanwhile, the operating

frequencies of CMRs are determined by lithographically defined IDT pitches, which enables monolithic multi-frequency resonators. However, the sidewall profile is a key factor for achieving high performance CMR devices [13,25,26].

Dry etching is a widely used process in group-III nitrides [27,28]. Pearton et al. [29] have studied the plasma etching of InN, GaN and other alloys. The importance of ICP etching profile has been reported. Chen et al. [30] have investigated the performance reduction of AlN lateral-field-excited (LFE) resonators caused by imperfect etching profile. Their study shows that when the profile is decreased from 90° to 60° , the electromechanical-coupling coefficient reduces from 1.9 to 1.4, due to the spurious mode by using finite element analysis (FEA) in COMSOL. Therefore, high performance CMRs require great ICP etching profile control. However, the ICP dry etching is a complex etching process with both chemical and physical reactions. How to optimize multiple etching process parameters remains a challenging problem to the society. A reliable ICP etching model based on $\text{Cl}_2/\text{BCl}_3/\text{N}_2$ mixture gases for AlN and AlScN ICP etching have not been well studied, as well as the AlN and AlScN ICP etching reaction mechanism. Therefore, a comprehensive analysis of multiple parameters in AlN and AlScN ICP etching is essential for deep understanding of AlN and AlScN piezoelectric thin film transducers.

In this paper, we have demonstrated the AlN and AlScN films ICP etching model using $\text{Cl}_2/\text{BCl}_3/\text{N}_2$ mixed gas. The mechanisms of ICP

* Corresponding authors at: School of Information Science and Technology, ShanghaiTech University, China.

E-mail addresses: luozhf@shanghaitech.edu.cn (Z. Luo), wutao@shanghaitech.edu.cn (T. Wu).

<https://doi.org/10.1016/j.mee.2021.111530>

Received 27 October 2020; Received in revised form 10 February 2021;

Available online 27 February 2021

0167-9317/© 2021 Elsevier B.V. All rights reserved.

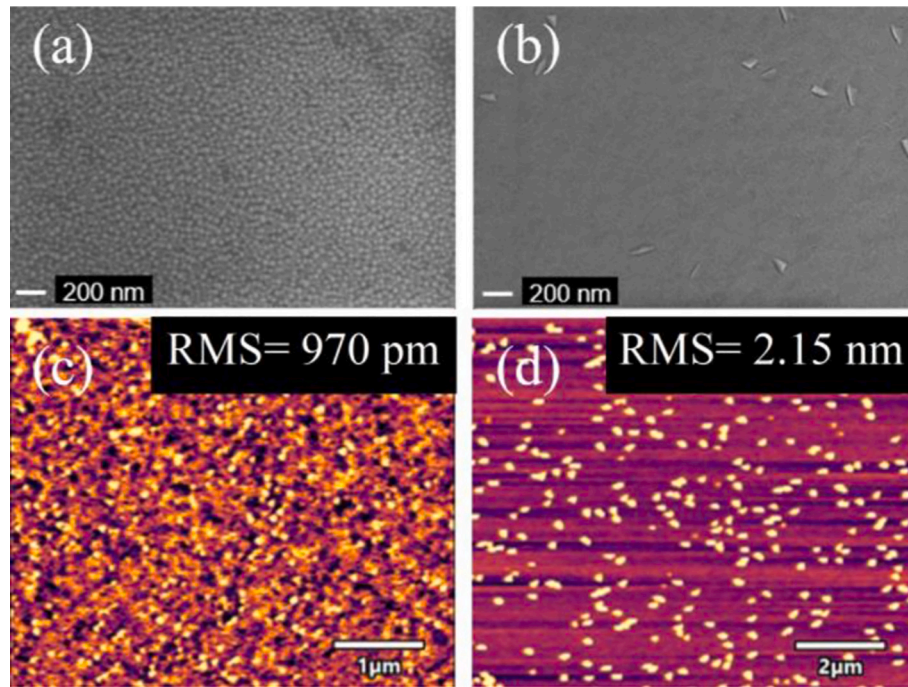


Fig. 1. SEM top view images of (a) (0002) oriented AlN surface, (b) (0002) oriented $\text{Al}_{0.94}\text{Sc}_{0.06}\text{N}$ surface; AFM height images of (c) (0002) oriented AlN surface, (d) (0002) oriented $\text{Al}_{0.94}\text{Sc}_{0.06}\text{N}$ surface.

power, RF power, flow rate of Cl_2 , BCl_3 and N_2 are analyzed. Then ICP etching recipes of AlN and AlScN films have been well optimized through an etching model to obtain the best etching profile. Finally, the fabrication and characterization of AlN CMRs with a high quality factor have been demonstrated using the optimized recipe.

2. Experiment

For the sample preparation, 1 μm (0002) polar AlN was deposited on Si wafer at 300 °C by reactive magnetron sputtering, while 0.5 μm (0002) polar $\text{Al}_{0.94}\text{Sc}_{0.06}\text{N}$ was also deposited on Si wafer at 300 °C by EVATEC CLN200 co-sputter system. The power of 4 inch Al and Sc targets are 1000 W and 150 W, respectively. The Sc concentration of the AlScN films was measured by energy dispersive X-ray spectrum (EDS) of Oxford AZtecOne system. The crystal orientation of AlN and $\text{Al}_{0.94}\text{Sc}_{0.06}\text{N}$ was investigated by X-ray diffraction (XRD) from PANalytical® Empyrean. The full width at half maximum (FWHM) of (0002) polar AlN thin film is around 1.2°, while the FWHM of (0002) polar $\text{Al}_{0.94}\text{Sc}_{0.06}\text{N}$ film is approximately 1.9°.

The surface morphology of AlN and $\text{Al}_{0.94}\text{Sc}_{0.06}\text{N}$ films was measured by scanning electron microscopy Carl Zeiss Gemini300, as shown in Fig. 1 (a) and (b), respectively. The surface roughness of AlN and $\text{Al}_{0.94}\text{Sc}_{0.06}\text{N}$ films was measured by Atomic Force Microscopy (Asylum Research Origin+). As shown in Fig. 1 (c) and (d), the RMS value R_a is 970 pm for AlN film and 2.15 nm for $\text{Al}_{0.94}\text{Sc}_{0.06}\text{N}$ film, respectively. The S1818 photoresist was spin-coated at 3000 rpm for 45 s as the etching mask. ICP dry etching of AlN and $\text{Al}_{0.94}\text{Sc}_{0.06}\text{N}$ films was performed using SENTECH SI-500 ICP etcher. The morphology of etching sidewall was measured by scanning electron microscopy Carl Zeiss Gemini300. Finally, the optimized etching recipe was implemented for AlN CMR device fabrication.

3. Results and discussion

3.1. AlN etching model

Rammal et al. [31] have reported a 0D plasma global model, in

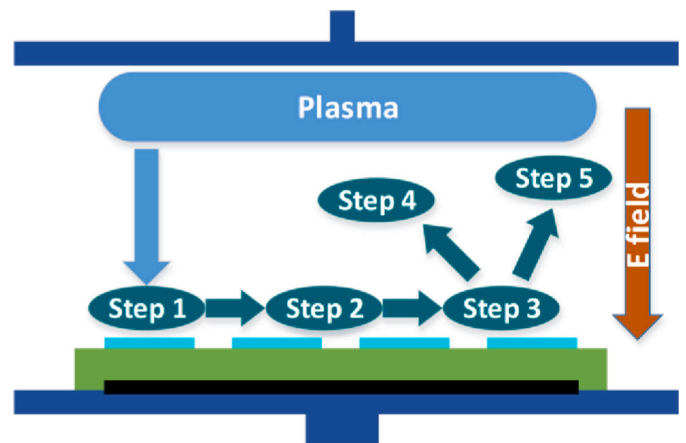
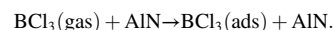
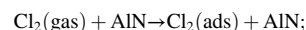


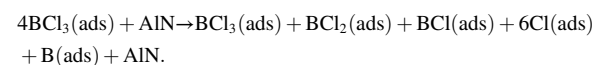
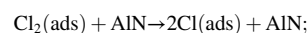
Fig. 2. Schematic of AlN ICP etching.

which the BCl_2 , BCl and B will be formed at the surface of the AlN from BCl_3 gas. Winters [32] proposes that plasma etching could be divided into five steps. According to their studies, we have adapted a similar model to describe our five-step plasma etching system of $\text{Cl}_2/\text{BCl}_3/\text{N}_2$ mixture AlN ICP etching as following (See Fig. 2.):

Step 1. Non-dissociative adsorption:



Step 2. Dissociative adsorption:



Step 3. Formation of product molecule:

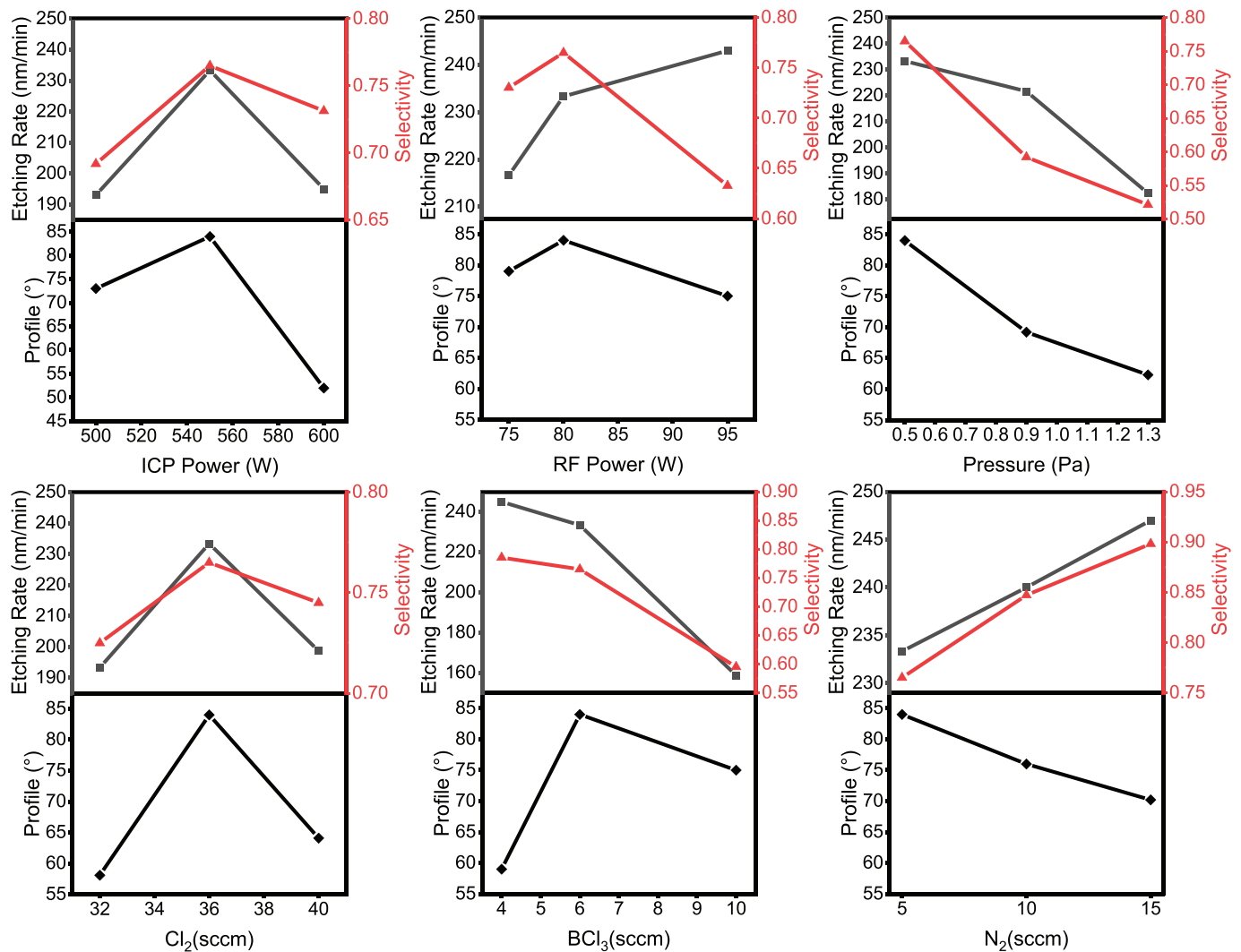
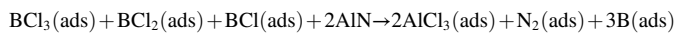
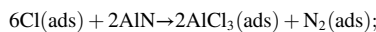
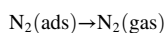
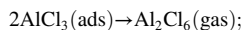


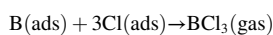
Fig. 3. (a) ICP etching rate, selectivity and profile versus the ICP power. (b) ICP etching rate, selectivity and profile versus the RF power. (c) ICP etching rate, selectivity and profile versus the pressure. (d) ICP etching rate, selectivity and profile versus the flow rate of Cl₂. (e) ICP etching rate, selectivity and profile versus the flow rate of BCl₃. (f) ICP etching rate, selectivity and profile versus the flow rate of N₂.



Step 4. Desorption of product molecule:



Step 5. Residue removal:



In step 1, Cl₂/BCl₃ in gas phase is non-dissociatively adsorbed at the AlN surface being etched. In step 2, Cl and BCl₂, BCl, Cl, B are generated by dissociative adsorption from Cl₂ and BCl₃, respectively. In step 3, BCl₃, BCl₂, BCl, Cl are etchants, which will react with the AlN at the surface being etched. AlCl₃, N₂ and B products are formed in these chemical reactions. Due to the strong oxidizing property of Cl, AlCl₃ will be generated at the AlN surface, while N³⁻ will be oxidized by Cl to generate N₂. It is known that N³⁻ cannot be oxidized to a positive valence like N³⁺, because product N₂ is so stable that oxidizing property of Cl is not enough. Due to the reducibility of N³⁻, some proportion of

B³⁺ is reduced to B²⁺, B⁺ and B. In step 4, one molecule Al₂Cl₆ dimer is formed by two molecule AlCl₃, because Al₂Cl₆ is more stable. In step 5, B residue on the surface will be desorbed into the gas phase by generating BCl₃.

3.2. AlN etching process optimization

ICP power is used to generate the plasma and control the number of high-energy reactive ions. According to the etching model, Cl₂ and BCl₃ with high energy are generated by high frequency electromagnetic field in the Cl₂/BCl₃/N₂ mixed gas etching system, and then they are accelerated to the surface of the AlN film being etched. In general, a larger ICP power can obtain a higher density of plasma, increasing the etching rate. In our experiment, as the ICP power is increased from 500 W to 550 W, the etching rate increases from 193 nm/min to 230 nm/min. This is because the etching system is in the reactant limited region when ICP power is set at 500 W. Increasing the ICP power will generate a higher concentration of Cl₂/BCl₃. These high density reactants will increase the possibility of contact with the AlN film. However, the etching rate decreases when ICP power is further increased to 600 W, because the plasma density probably reaches saturation, and higher plasma density could promote polymer redeposition on the surface of AlN films, such as AlCl₃; therefore, the etching rate drops at the ICP power of 600 W, as

shown in Fig. 3 (a). The selectivity (the etching rate of the AlN relative to the S1818 photoresist mask) has a similar trend. The chemical reactions are dominant in the AlN etching process, therefore a higher etching rate could also achieve a better selectivity. However, once the ICP power reaches saturation, like 600 W in our case, the redeposition or polymer formation will limit the chemical reaction contribution. In the meanwhile, more N_2 and BCl_3 reach the surface and promote the physical bombardment, which leads to a poor selectivity, as shown in Fig. 3 (a). When the ICP power is 500 W, the etching is in reactant limited region, a relatively low etching rate and a poor etching profile are obtained. As the ICP power increases to the 550 W, the etching profile reaches nearly 85° , which attributes to the higher concentration of reactants Cl_2/BCl_3 and more powerful physical bombardment of BCl_3/N_2 . However, since the plasma density generated at the ICP power of 600 W is much higher, polymer redeposition would limit the chemical etching process, thereby reducing the etching rate and volatilization rate, as well as the profile, as indicated in Fig. 3 (a).

RF power plays another key factor for controlling the plasma bombardment energy to the sample. As shown in Fig. 3 (b), as the RF power increases from 75 W to 95 W, the kinetic energy of $Cl_2/BCl_3/N_2$ increases. In this case, Cl_2/BCl_3 mixture gas with higher energy would increase the possibility of Al–N bond breaking and Cl_2/BCl_3 bombardment at the surface of AlN being etched, so that the etching rate increases. On the other hand, due to the exothermic reaction and physical bombardment, a higher RF power would increase the temperature of the etched surface, which could promote the generation of Al_2Cl_6 dimers from $AlCl_3$ molecule, which would desorb more easily from the surface. Therefore, both chemical and physical processes are enhanced. As for selectivity, when RF power is increased from 75 W to 80 W, the selectivity slightly increases to 0.76 as the possibility of breaking Al–N bonds increases. Unfortunately, due to the strong kinetic energy of $Cl_2/BCl_3/N_2$, physical bombardment is much stronger under 95 W RF power. The chemical etching of AlN does not change much, however, the etching rate for the photoresist becomes larger, leading to a significant drop on the selectivity. As for the profile, the best sidewall slope is obtained under 80 W RF power. Similar to the trend of selectivity, the profile becomes much worse. It can be seen from the Fig. 3(b) that rate of increase of the etching rate decreases. Through our etching model, in step 3, more $AlCl_3$ molecules and B radicals are generated on the surface due to a higher RF power. However, despite the enhancement of physical bombardment, a large number of molecule products cannot be desorbed in time, which leads to a much poorer etching profile.

The influence of the reaction pressure has been studied as well, since the chamber pressure determines the mean free path of the reactants. As the pressure increases, the mean free path of the plasma $Cl_2/BCl_3/N_2$ reduces, but the possibility of plasma collision increases, which means the directionality of the movement is decreased, and it would be more difficult for the chemical reactants to reach the AlN surface. On the other hand, due to the reduction of the kinetic energy of plasma, the chemical reactions become more difficult even if the plasma reaches the AlN surface. Therefore, the etching rate of AlN film drops while increasing the reaction pressure as shown in Fig. 3 (c). As for selectivity, it keeps decreasing from 0.75 to 0.52. The AlN is hard to be etched through chemical process, so that the chemical etching is limited, and the physical bombardment is relatively weak. As for profile, it changes from greater than 84° to approximately 62° from 0.5 Pa to 1.3 Pa, as shown in Fig. 3 (c). The higher pressure will also lead to redeposition and formation of polymer, because such relatively low energy BCl_3/N_2 cannot effectively desorb the products $AlCl_3$ and B into the vapor phase, the ICP etching tends to be isotropic.

The influence of Cl_2 , BCl_3 and N_2 gases has been studied and analyzed in Figs. 3 (d-f). According to the etching model, after Cl_2 gas is absorbed at the AlN surface, it can react with AlN and produce $AlCl_3$ effectively. As shown in Fig. 3 (d), as for etching rate and selectivity, they both go up as the flow rate of Cl_2 gas increases from 32 sccm to 36

Table 1
Influence of AlN ICP Etching parameters.

Parameters	Etching Rate (nm/min)	Selectivity
RF Power	↑	–
Pressure	↓	↓
BCl_3	↓	↓
N_2	↑	↑

↑ Indicates an increase in value, ↓ indicates a decrease in value.

sccm. However, they do not further increase as the Cl_2 flow rate continues to increase. The product $AlCl_3$ generated in such chemical reaction will be redeposited on the AlN surface, and with a higher proportion of Cl_2 , the efficiency of desorbing the $AlCl_3$ into the gas phase becomes lower, which would limit further reactions, therefore the etching rate drops under 36 sccm Cl_2 flow rate. As for profile, as shown in Fig. 3 (d), when the flow rate of Cl_2 gas is increased to 36 sccm, the best profile can be obtained due to an optimal chemical etching rate, while Al_2Cl_6 can be generated from $AlCl_3$ efficiently by physical bombardment. However, the anisotropic etching is limited by the redeposition on the surface, so the profile becomes much worse.

Compared to Cl_2 gas, the reaction rate of BCl_3 and AlN is slow. According to steps 2 and 3 in the etching model, BCl_3 needs to be dissociated into BCl_2 , BCl and Cl, then they react with AlN, respectively. On the one hand, due to the oxidizing property, the reaction rate of BCl_3 , BCl_2 and BCl with AlN is slower than that of Cl. On the other hand, the product B generated by the etchants BCl_3 , BCl_2 and BCl will be redeposited on the surface being etched. This multi-step chemical reaction makes BCl_3 decrease the total etching rate, because the presence of such gas will occupy certain areas of the AlN surface, where the etching rate is much lower than the area occupied by the Cl_2 gas. However, the BCl_3 can etch oxide layer quickly by strong physical bombardment and $AlCl_3$ as well, which means a certain amount of BCl_3 can increase the total etching rate, because the Cl_2 gas can hardly etch the Al_2O_3 , regardless of physical or chemical processes, as shown in Fig. 3 (e). The selectivity has the same tendency as the etching rate, because the chemical reaction is limited, as shown in Fig. 3 (e). As for the profile, it can be seen from Fig. 3 (e) that because flow rate of 6 sccm BCl_3 is better to efficiently desorb the product, the profile reaches greater than 84° . With a higher flow rate, the proportion of BCl_3 is too large, which reduces the profile to about 75° .

N_2 gas acts as the physical bombard gas. The increase in flow rate of N_2 will enhance the physical etching process. On one hand, more N_2 results in a better dissociation of BCl_3 to generate BCl_2 , BCl and Cl, which means it can increase the density of etchant. On the other hand, the strong physical bombardment of N_2 could promote the product desorption into gas phase and reduce the effects of redeposition and

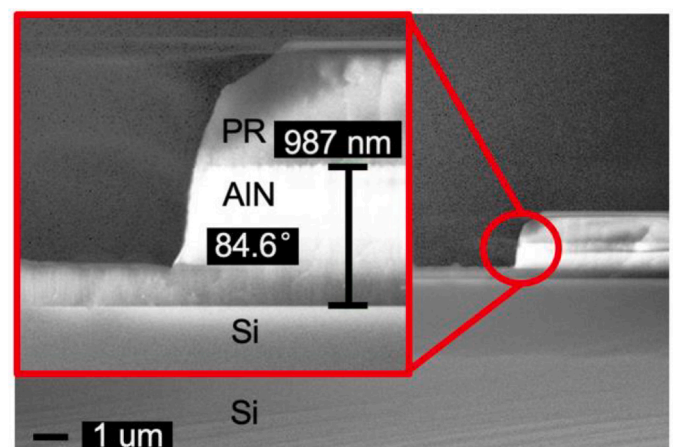


Fig. 4. SEM cross-section view of AlN etching results with photoresist mask.

Table 2
ICP etching characteristics of etching AlN.

Work	Mask	ICP (W)	RF Power/Voltage	Pressure	Etching Gas	Etching Rate (nm/min)	Profile (°)
[25]	Ni	500	-310 V	2 mTorr	Cl ₂ /BCl ₃ /Ar	176	80.1
[33]	SiO ₂	700	80 W	0.5 Pa	Cl ₂ /BCl ₃ /Ar	77.5	83
[30]	Photoresist	NA	NA	NA	Cl ₂ based	NA	60
[26]	SiN _x	500	100 W	0.5 Pa	Cl ₂ /BCl ₃ /Ar	750	NA
[28]	NA	500	-83 V	10 mTorr	Cl ₂ /BCl ₃ /O ₂	90	NA
Ours	Photoresist	550	80 W	0.5 Pa	Cl ₂ /BCl ₃ /N ₂	230	> 84

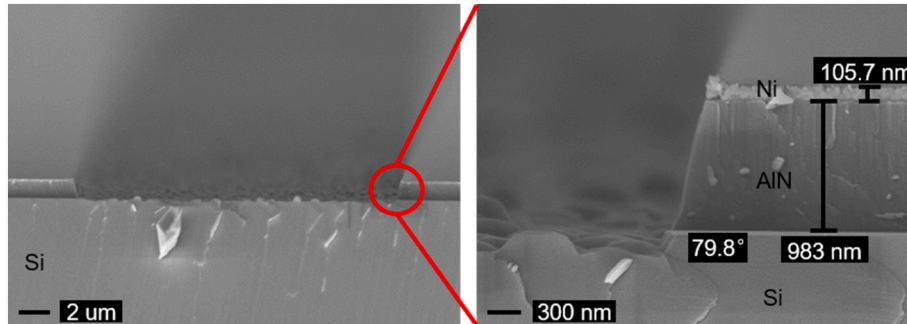


Fig. 5. SEM cross-section view of AlN etching results with Ni mask.

polymer formation. These two aspects show that N₂ can not only enhance chemical reactions, but also strengthen physical bombardment, as shown in Fig. 3 (f). Although the heavier molecular is a better choice for achieving a higher etching rate, selectivity is also a significant factor in ICP etching, especially for fabricating the AlN CMR. Since the physical bombardment efficiency of nitrogen is lower than that of argon, the selectivity of the etching with nitrogen is better compare to argon, however, it is undeniable that nitrogen would slightly reduce the etching rate. As shown in Fig. 3 (f), the profile decreases from 84° to 70°, since it is difficult to control the directionality under higher etching rates with a high ratio of N₂.

Table 1 gives the influence of different etching parameters. It has shown that etching rate has the same relationship with RF power. Etching rate and selectivity have a positive correlation with flow rate of N₂, while they have opposite relationships with flow rate of BCl₃ and pressure.

Fig. 4 illustrates an AlN etching profile with over 84° sidewall using the optimized etching recipe at 550 W ICP power, 80 W RF power, the Cl₂/BCl₃/N₂ flow rate of 36/6/5 sccm, respectively. Table 2 shows the comparison of etching rate and profile of AlN ICP etching with other works. In most AlN-based piezoelectric thin film transducers, the thickness of piezoelectric layer would not be too thin or too thick, generally between 0.2 μm to 2 μm. In this situation, the etch rate of 230 nm/min is a reasonable number. J. Yang *et al.* [33] have reported an AlN ICP etching recipe of 77.5 nm/min and 83° etching profile. Although it has similar profile, the etching rate might be slow for applications requiring thicker film. A. P. Shah *et al.* [26] reported a high etching rate recipe of 750 nm/min in (11–22) semi polar AlN. However, they did not show the etching profile, and such semi polar AlN cannot be used as piezoelectric transducers due to low d₃₃. Our optimized AlN ICP etching recipe can achieve the best etching profile with a reasonable etching rate for a variety of applications.

3.3. Ni mask sample etching

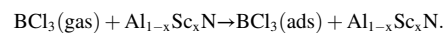
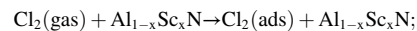
In order to verify the good compatibility of the recipe demonstrated in the previous section. A 150 nm Ni layer deposited by electron beam evaporation system is used as the etching mask. It can be seen from Fig. 5 that the profile is nearly 80°, while the selectivity is greater than 30 (the etching rate of the AlN relative to the etching rate of Ni mask). Such a

good profile and selectivity indicate that it is a promising method for device manufacturing using Ni as both the etching mask and top electrode.

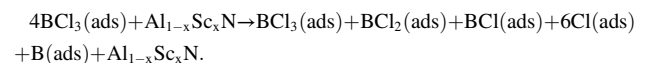
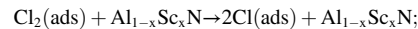
3.4. AlScN etching model

AlScN dry etching is a critical problem in fabrication of AlScN film based transducers. In order to analyze the AlScN ICP etching reaction mechanism, the Cl₂/BCl₃/N₂ mixed gas etching can be described by the following five-step plasma etching model:

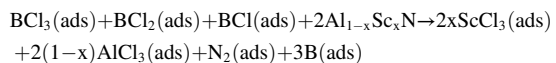
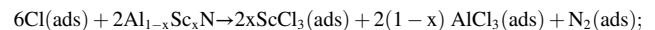
Step 1. Non-dissociative adsorption:



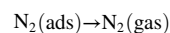
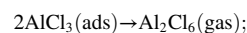
Step 2. Dissociative adsorption:



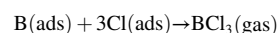
Step 3. Formation of product molecule:



Step 4. Desorption of product molecule:



Step 5. Residue removal:



Similar to the first two steps of the AlN etching model, Cl₂/BCl₃ in gas phase is non-dissociatively adsorbed at the surface of AlScN films.

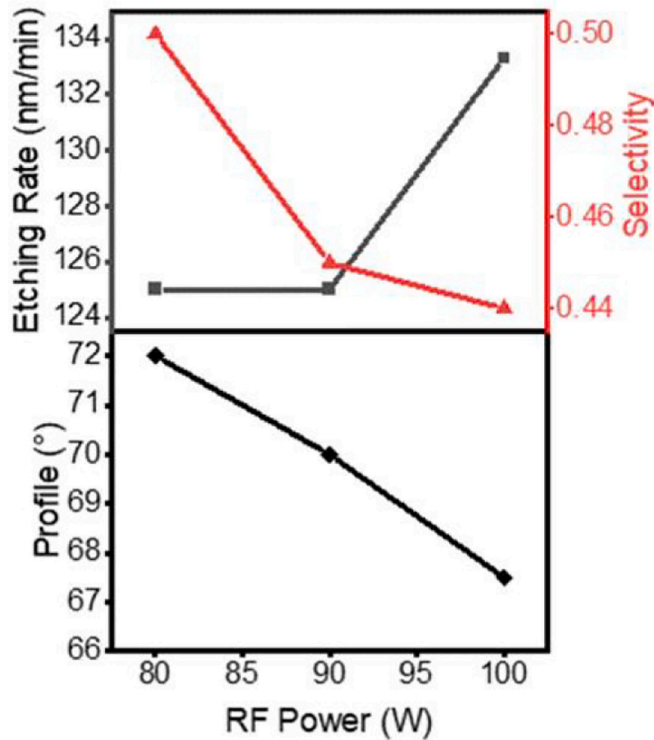


Fig. 6. ICP etching rate, selectivity and profile versus RF Power.

Then Cl_2 is dissociatively adsorbed into Cl, while BCl_3 is adsorbed into BCl_2 , BCl , Cl , B respectively. In step 3, BCl_3 , BCl_2 , BCl , Cl will react with $\text{Al}_{1-x}\text{Sc}_x\text{N}$ at the surface being etched. The products of the chemical reaction are ScCl_3 and AlCl_3 . ScCl_3 is an ionic compound, which is less volatile than AlCl_3 . The sublimation temperature of ScCl_3 is about 900 degree Celsius, but only 100 degree Celsius for AlCl_3 . Moreover, AlCl_3 , ScCl_3 , N_2 and B by-products are generated due to the oxidizing property of Cl . In step 4, gas phase Al_2Cl_6 dimers are generated. Since the sublimation temperature of ScCl_3 is very high, covalent ScCl_3 is difficult to be desorbed into the gas phase, which will remain at the surface being etched. Only the high energy physical bombardment can make ScCl_3 leave the surface. In step 5, residue B will be desorbed into the gas by generating BCl_3 .

3.5. AlScN etching process optimization

RF power can control the energy of the plasma bombarding to the sample. With increasing the RF power from 80 W to 100 W, the energy of $\text{Cl}_2/\text{BCl}_3/\text{N}_2$ plasma bombarding to the $\text{Al}_{0.94}\text{Sc}_{0.06}\text{N}$ sample increases. Such higher energy can increase the possibility of Al-N and Sc-N bond

breaking by chemical reactions. According to the AlScN etching model, the generating rate of ScCl_3 and AlCl_3 will increase in step 3. At the same time, the BCl_3/N_2 will reach the $\text{Al}_{0.94}\text{Sc}_{0.06}\text{N}$ surface easier, which can enhance the physical bombardment, so that the products ScCl_3 will be removed from surface faster and then the etching rate will increase. However, the increase of RF power will significantly enhance the kinetic energy of heavy plasma, like BCl_3 and N_2 , the selectivity will be decreased, as shown in Fig. 6. As for the profile, its tendency is similar to the selectivity. The sidewall angle is above 70° at RF power 80 W, and then decreases to 67.5° , due to the too strong physical bombardment by BCl_3/N_2 .

It can be seen from Fig. 7 that the optimized profile is higher than 77° , while the etching surface is very smooth and clean. Our optimized etching recipe is 550 W ICP power, 80 W RF power and the flow rate of $\text{Cl}_2/\text{BCl}_3/\text{N}_2$ are 15/30/5 sccm, respectively.

3.6. AlN CMR device fabrication

AlN lateral field excitation (LFE) contour-mode resonators (CMRs) were fabricated using a traditional 4-mask process.

The fabrication process flow is shown in Fig. 8. Starting from a high-resistive (100) silicon wafer, the bottom electrode of 10 nm Ti/100 nm Pt was patterned by physical vapor deposition (PVD) through a lift-off process. Then, 1 μm piezoelectric layer was deposited using EVATEC CLN200 magnetron sputtering system. After that, 200 nm Al was deposited and patterned as the top electrode via a lift-off process. Then, the optimized ICP etching step was used to define the shape of the CMRs, using S1818 photoresist as the etching mask. The last step was to release the resonator via. The device was released by XeF_2 etching and characterized using Keysight® N5234B network analyzer.

As shown in Fig. 9, a 4-finger lateral-field-excited (LFE) AlN contour-mode resonator (CMR) with $\lambda = 20 \mu\text{m}$ and $L = 170 \mu\text{m}$ is fabricated with a resonance of approximately 400 MHz and a quality factor of over 1600.

4. Conclusion

In this paper, we have investigated the ICP etching characteristics of AlN and $\text{Al}_{0.94}\text{Sc}_{0.06}\text{N}$ piezoelectric thin films. By optimizing the parameters of Cl_2 , BCl_3 and N_2 flow rates, pressure, RF power and ICP power, a nearly vertical profile angle of 84° is obtained at AlN thin films, with a desirable etching rate of approximately 230 nm/min, and a selectivity of 0.77:1 relative to S1818 photoresist. Meanwhile, the same AlN thin film with Ni mask is also investigated to analyze the compatibility. A profile of nearly 80° and a selectivity over 30 are achieved. The etching performance is analyzed through a 5-step model and optimized etching profile is evaluated with AlN piezoelectric resonator device fabrication. A 4-finger AlN LFE CMR is fabricated and characterized with operating resonance at 400 MHz and a high Q exceeding 1600.

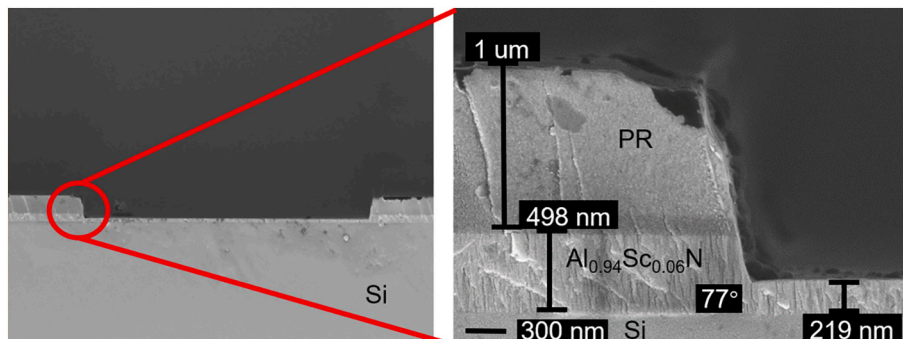


Fig. 7. SEM cross-section view of $\text{Al}_{0.94}\text{Sc}_{0.06}\text{N}$ etching results with photoresist mask.

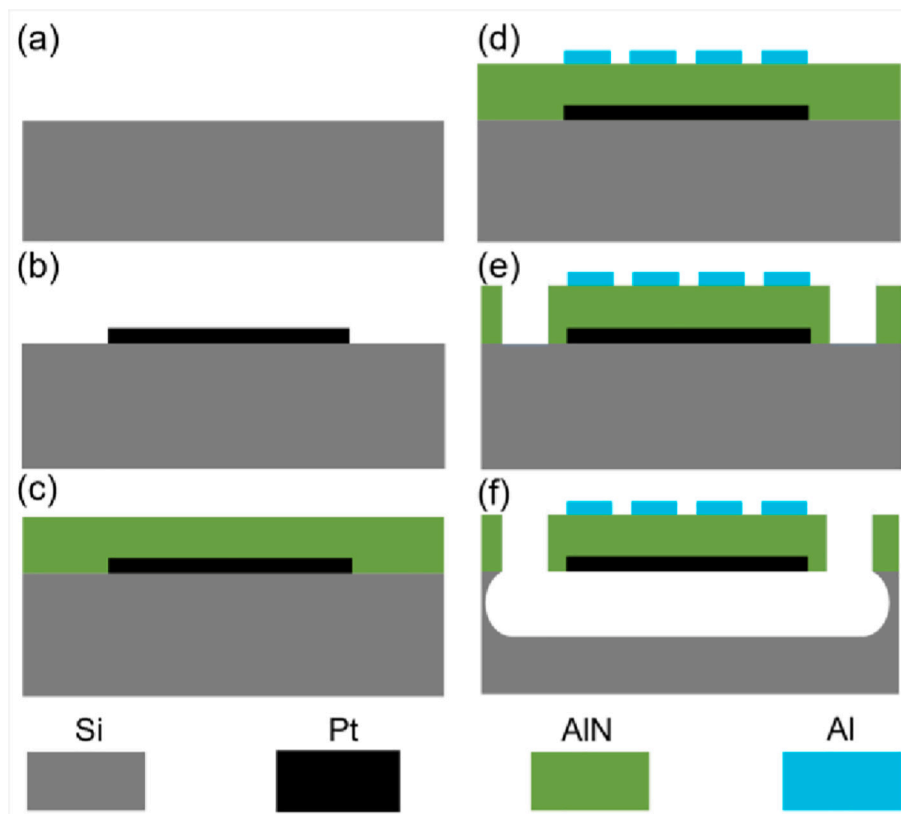


Fig. 8. (a) Starting with a high-resistive Si wafer. (b) Lift-off the Ti/Pt layer as the bottom electrode on 4-in. silicon wafer. (c) Deposit AlN piezoelectric layer. (d) Lift-off the Al layer as top electrode. (e) ICP dry etching. (f) Release the CMRs through XeF₂.

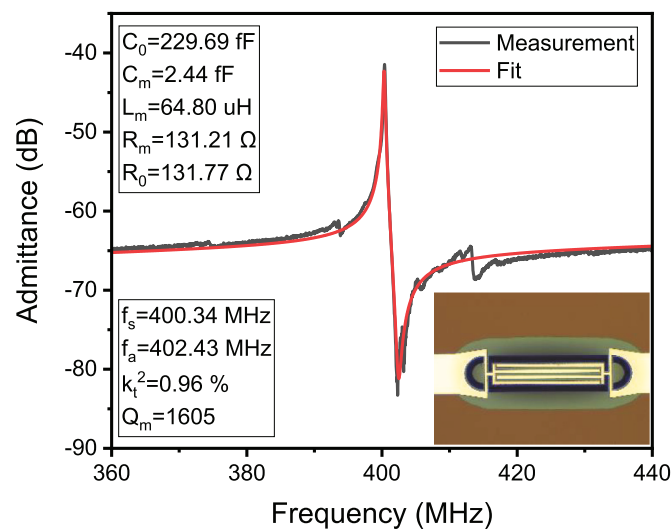


Fig. 9. The admittance response of AlN CMR. Measured admittance data is in black line, and the fitted admittance is in red line; the inset is an optical microscopy top view of the fabricated AlN CMR.

Declaration of Competing Interest

None.

Acknowledgements

The authors appreciate the support from the ShanghaiTech Quantum Device Lab (SQDL), and Analytical Instrumentation Center (SPSTAIC10112914) XRD Lab, School of Physical Sciences and

Technology, ShanghaiTech University, Natural Science Foundation of Shanghai (19ZR1477000) and National Natural Science Foundation of China (61874073).

References

[1] J. Wang, Z. Ren, C.-C. Nguyen, 1.156-GHz self-aligned vibrating micromechanical disk resonator, *IEEE Trans. Ultrason. Ferroelectr. Freq. Control* 51 (12) (2004) 1607–1628.

- [2] S. Pourkamali, A. Hashimura, R. Abdolvand, G.K. Ho, A. Erbil, F. Ayazi, High-Q single crystal silicon HARPSS capacitive beam resonators with self-aligned sub-100-nm transduction gaps, *J. Microelectromech. Syst.* 12 (4) (2003) 487–496.
- [3] L.-W. Hung, C.T.-C. Nguyen, Capacitive-piezoelectric AlN resonators with $Q > 12,000$, in: 2011 IEEE 24th International Conference on Micro Electro Mechanical Systems, 2011, pp. 173–176.
- [4] G. Piazza, P.J. Stephanou, A.P. Pisano, Piezoelectric aluminum nitride vibrating contour-mode MEMS resonators, *J. Microelectromech. Syst.* 15 (6) (Dec. 2006) 1406–1418.
- [5] G.L. Smith, J.S. Pulskamp, L.M. Sanchez, D.M. Potrepka, R.M. Proie, T.G. Ivanov, R.Q. Rudy, W.D. Nothwang, S.S. Bedair, C.D. Meyer, R.G. Polcawich, PZT-based piezoelectric MEMS technology, *J. Am. Ceram. Soc.* 95 (6) (Jun. 2012) 1777–1792.
- [6] R. Ruby, 11E-2 Review and Comparison of Bulk Acoustic Wave FBAR, SMR Technology, in: 2007 IEEE Ultrasonics Symposium Proceedings, New York, NY, Oct. 2007, pp. 1029–1040.
- [7] T. Wu, G. Chen, C. Cassella, W.Z. Zhu, M. Assylbekova, M. Rinaldi, N. McGruer, Design and fabrication of AlN RF MEMS switch for near-zero power RF wake-up receivers, in: 2017 IEEE SENSORS, Glasgow, Oct. 2017, pp. 1–3.
- [8] A. Gao, K. Liu, J. Liang, T. Wu, AlN MEMS filters with extremely high bandwidth widening capability, *Microsyst. Nanoeng.* 6 (1) (Dec. 2020) 74.
- [9] S. Gong, G. Piazza, Design and analysis of Lithium-Niobate-based high electromechanical coupling RF-MEMS resonators for wideband filtering, *IEEE Trans. Microw. Theory Tech.* 61 (1) (Jan. 2013) 403–414.
- [10] M. Schreiter, R. Gabl, D. Pitzer, R. Primig, W. Wersing, Electro-acoustic hysteresis behaviour of PZT thin film bulk acoustic resonators, *J. Eur. Ceram. Soc.* 24 (6) (Jan. 2004) 1589–1592.
- [11] Q.-X. Su, P. Kirby, E. Komuro, M. Imura, Q. Zhang, R. Whatmore, Thin-film bulk acoustic resonators and filters using ZnO and lead-zirconium-titanate thin films, *IEEE Trans. Microw. Theory Tech.* 49 (4) (Apr. 2001) 769–778.
- [12] G. Piazza, P.J. Stephanou, A.P. Pisano, Single-Chip multiple-frequency ALN MEMS filters based on contour-mode piezoelectric resonators, *J. Microelectromech. Syst.* 16 (2) (Apr. 2007) 319–328.
- [13] M.-H. Li, C.-Y. Chen, R. Lu, Y. Yang, T. Wu, S. Gong, Power-Efficient Ovenized Lithium Niobate SHO Resonator Arrays with Passive Temperature Compensation, in: 2019 IEEE 32nd International Conference on Micro Electro Mechanical Systems (MEMS), Seoul, Korea (South), Jan. 2019, pp. 911–914.
- [14] M. Akiyama, K. Kano, A. Teshigahara, Influence of growth temperature and scandium concentration on piezoelectric response of scandium aluminum nitride alloy thin films, *Appl. Phys. Lett.* 95 (16) (2009) 162107.
- [15] C. Caliendo, P. Imperatori, High-frequency, high-sensitivity acoustic sensor implemented on ALN/Si substrate, *Appl. Phys. Lett.* 83 (8) (Aug. 2003) 1641–1643.
- [16] J.G. Rodriguez-Madrid, G.F. Iriarte, J. Pedros, O.A. Williams, D. Brink, F. Calle, Super-high-frequency SAW resonators on AlN/diamond, *IEEE Electron Device Lett.* 33 (4) (Apr. 2012) 495–497.
- [17] H.P. Loeb, M. Klee, C. Metzmacher, W. Brand, R. Milsom, P. Lok, Piezoelectric thin AlN films for bulk acoustic wave (BAW) resonators, *Mater. Chem. Phys.* 79 (2–3) (Apr. 2003) 143–146.
- [18] G. Wingqvist, AlN-based sputter-deposited shear mode thin film bulk acoustic resonator (FBAR) for biosensor applications — a review, *Surf. Coat. Technol.* 205 (5) (Nov. 2010) 1279–1286.
- [19] Jun-Phil Jung, Jin-Bock Lee, Myung-Ho Lee, Jin-Seok Park, Experimental and theoretical investigation on the relationship between AlN properties and AlN-based FBAR characteristics, in: IEEE International Frequency Control Symposium and PDA Exhibition Jointly with the 17th European Frequency and Time Forum, 2003. Proceedings of the 2003, Tampa, FL, USA, 2003, pp. 779–784.
- [20] S.I. Jung, C. Ryu, G. Piazza, H.J. Kim, A study on the effects of bottom electrode designs on aluminum nitride contour-mode resonators, *Micromachines* 10 (11) (Nov. 2019) 758.
- [21] M. Giovannini, S. Yazici, N.-K. Kuo, G. Piazza, Apodization technique for spurious mode suppression in AlN contour-mode resonators, *Sensors Actuators A Phys.* 206 (Feb. 2014) 42–50.
- [22] C. Zuniga, M. Rinaldi, G. Piazza, Quality factor of MEMS and NEMS AlN Contour Mode Resonators in liquid media, in: 2009 IEEE International Ultrasonics Symposium, Rome, Italy, Sep. 2009, pp. 2568–2571.
- [23] M. Rinaldi, C. Zuniga, Zuo Chengjie, G. Piazza, Super-high-frequency two-port AlN contour-mode resonators for RF applications, *IEEE Trans. Ultrason. Ferroelectr. Freq. Control* 57 (1) (Jan. 2010) 38–45.
- [24] T. Wu, Z. Qian, M. Rinaldi, Low cost thin film encapsulation for AlN resonators, in: 2018 IEEE Micro Electro Mechanical Systems (MEMS), Belfast, Jan. 2018, pp. 1024–1027.
- [25] X. Liu, C. Sun, B. Xiong, L. Niu, Z. Hao, Y. Han, Y. Luo, Smooth etching of epitaxially grown AlN film by Cl₂/BCl₃/Ar-based inductively coupled plasma, *Vacuum* 116 (Jun. 2015) 158–162.
- [26] A.P. Shah, A.A. Rahman, A. Bhattacharya, ICP-RIE etching of polar, semi-polar and non-polar AlN: comparison of Cl₂/Ar and Cl₂/BCl₃/Ar plasma chemistry and surface pretreatment, *Semicond. Sci. Technol.* 30 (1) (Jan. 2015) 015021.
- [27] S.J. Pearton, R.J. Shul, F. Ren, A review of dry etching of GaN and related materials, *MRS Internet J. Nitride Semicond. Res.* 5 (1) (2000) e11.
- [28] F. Engelmark, G.F. Iriarte, I.V. Katardjiev, Selective etching of Al/AlN structures for metallization of surface acoustic wave devices, *J. Vac. Sci. Technol. B Microelectron. Nanometer Struct. Process. Meas. Phenom.* 20 (3) (2002) 843–848.
- [29] S.J. Pearton, C. Kuo, GaN and related materials for device applications, *MRS Bull.* 22 (2) (Feb. 1997) 17–21.
- [30] G. Chen, F. Pop, M. Rinaldi, “Super high frequency lateral-field-excited aluminum nitride cross-sectional lamé mode resonators,” in 2019 20th International Conference on Solid-State Sensors, Actuators and Microsystems & Eurosensors XXXIII (TRANSDUCERS & EUROSENSORS XXXIII), Berlin, Germany, Jun. 2019, pp. 539–542.
- [31] M. Rammal, A. Rhallabi, D. Néel, D. Make, A. Shen, A. Djouadi, AlN etching under ICP cl₂/BCl₃/Ar plasma mixture: experimental characterization and plasma kinetic model, *MRS Adv.* 4 (27) (2019) 1579–1587.
- [32] H.F. Winters, The role of chemisorption in plasma etching, *J. Appl. Phys.* 49 (10) (Oct. 1978) 5165–5170.
- [33] J. Yang, C. Si, G. Han, M. Zhang, L. Ma, Y. Zhao, J. Ning, Researching the aluminum nitride etching process for application in MEMS resonators, *Micromachines* 6 (2) (Feb. 2015) 281–290.